JOURNAL OF GEOPHYSICAL RESEARCH, VOL. 114, A03212, doi:10.1029/2008JA013776, 2009

Propagation of unducted whistlers from their source lightning: A case study

O. Santolík,[1,2,3] M. Parrot,[4,5] U. S. Inan,[6] D. Burešová,[7] D. A. Gurnett,[1] and J. Chum[7]

Received 29 September 2008; revised 10 December 2008; accepted 15 January 2009; published 24 March 2009.

[1] We analyze nightside measurements of the DEMETER spacecraft related to lightning activity. At the 707 km altitude of DEMETER, we observe 3-D electric and magnetic field waveforms of fractional-hop whistlers. At the same time, the corresponding atmospherics are recorded by a very low frequency (VLF) ground-based station located in Nançay (France). The source lightning strokes are identified by the METEORAGE lightning detection network. We perform multidimensional analysis of the DEMETER measurements and obtain detailed information on wave polarization characteristics and propagation directions. This allows us for the first time to combine these measurements with ray-tracing simulation in order to directly characterize how the radiation penetrates upward through the ionosphere. We find that penetration into the ionosphere occurs at nearly vertical wave vector angles (as was expected from coupling conditions) at distances of 100–900 km from the source lightning. The same distance is traveled by the simultaneously observed atmospherics to the VLF ground station. The measured dispersion of fractional-hop whistlers, combined with the ionosonde measurements at the Ebro observatory in Spain, allows us to derive the density profile in the topside ionosphere.

Citation: Santolík, O., M. Parrot, U. S. Inan, D. Burešová, D. A. Gurnett, and J. Chum (2009), Propagation of unducted whistlers from their source lightning: A case study, *J. Geophys. Res.*, *114*, A03212, doi:10.1029/2008JA013776.

1. Introduction

[2] During the 55 years since the pioneering work of *Storey* [1953] a number of studies have been published concerning the generation, propagation, and effects of lightning-generated whistlers in the Earth's ionosphere and magnetosphere (see, e.g., reviews by *Sazhin et al.* [1992] and *Helliwell* [1993]). Observations of whistlers significantly contributed to the early remote investigation of the Earth's plasma environment [*Crary et al.*, 1956; *Helliwell et al.*, 1956; *Smith and Carpenter*, 1961; *Carpenter*, 1963]. Whistlers have been then subsequently discovered also in the Jovian and Kronian magnetospheres [*Gurnett et al.*, 1979; *Akalin et al.*, 2006], and generated controversy in the case of Venus [*Gurnett et al.*, 2001; *Russell et al.*, 2007].

[3] In spite of this long history, terrestrial whistlers still attract active research, for example in connection with lightning-induced precipitation of energetic electrons [*Peter and Inan*, 2004, 2007; *Bortnik et al.*, 2006; *Inan et al.*, 2007], with propagation of whistlers in magnetospheric density structures and ducts [*McCormick et al.*, 2002; *Platino et al.*, 2005; *Pasmanik and Trakhtengerts*, 2005], with loss processes in the Van Allen radiation belts [*Bortnik et al.*, 2003; *Rodger et al.*, 2003], with the dynamics of the slot region [*Meredith et al.*, 2007], and with the still controversial question of the origin of plasmaspheric hiss [*Sonwalkar and Inan*, 1989; *Draganov et al.*, 1992; *Green et al.*, 2005, 2006; *Thorne et al.*, 2006; *Bortnik et al.*, 2008].

[4] One of the unresolved problems is how the whistlers penetrate through the ionosphere. In the Earth-ionosphere wave-guide, the electromagnetic wave induced by lightning currents propagates as a broadband pulse, an atmospheric [*Helliwell*, 1965, p. 78], showing sometimes cutoffs and dispersive effects ("tweeks", analyzed recently, e.g., by *Ferencz et al.* [2007]). The isotropic atmospheric propagation at speeds close to the speed of light is very different from anisotropic propagation with much lower phase speeds (large wave numbers) in the ionosphere. In a simplified approach, assuming that the propagation properties vary in the vertical direction, horizontal wave vector components stay constant at the interface between the Earth-ionosphere waveguide and the ionosphere. On the ionospheric side of this interface we thus obtain a narrow transmission cone of wave vector directions close to the vertical [*Helliwell*, 1965, p. 53].

[5] In reality, this interface may be much more complex. Some results [e.g., *James*, 1972] indicate that the large-scale density inhomogeneities in the ionosphere can shift the

[1]Department of Physics and Astronomy, University of Iowa, Iowa City, Iowa, USA.
[2]Permanently at Department of Space Physics, Institute of Atmospheric Physics, Prague, Czech Republic.
[3]Permanently at Faculty of Mathematics and Physics, Charles University, Prague, Czech Republic.
[4]Laboratoire de Physique et Chimie de l'Environnement, CNRS, Orleans, France.
[5]University of Orléans, Orleans, France.
[6]Space, Telecommunications and Radioscience Laboratory, Stanford University, Stanford, California, USA.
[7]Department of Aeronomy, Institute of Atmospheric Physics, Prague, Czech Republic.

0148-0227/09/2008JA013776$09.00

wave vector directions toward the local direction of the Earth's magnetic field ($\mathbf{B}_0$). Direct ionospheric measurements of wave vector directions of downgoing whistlers by a rocket experiment [*Iwai et al.*, 1974] yielded contradictory results, with wave vector directions widely distributed around a broad peak at $\approx 20^\circ$ with respect to the vertical and at $\approx 40^\circ$ with respect to $\mathbf{B}_0$. More recently, *Karlsson et al.* [2005] analyzed multicomponent measurements of a low-orbiting spacecraft. They found that the normal to the polarization plane of a whistler precesses around the geomagnetic field which again seems to be inconsistent with a simple ionospheric propagation pattern.

[6] Concerning the size of the region through which the energy penetrates into the ionosphere, it was experimentally found already by *Storey* [1953, p. 118] that "whistlers are produced by waves which originate in a lightning flash and return, after some time, to an area of radius about 2000 km in the neighbourhood of the original flash." However, ground-based measurements cannot resolve if this radius results from (1) the initial penetration of waves upward into the ionosphere, (2) propagation of whistlers in the magnetosphere, or (3) their penetration back downward into the atmosphere. Some studies assume, that the penetration of the upward propagating waves happens over roughly the same area as for the whistlers penetrating back downward [e.g., *Ohta et al.*, 1994]. This would mean that atmospherics can travel up to thousands of kilometers from the source lightning in the Earth-ionosphere waveguide before a part of their energy enters into the ionosphere and forms a whistler. This assumption has been supported by direct rocket measurements of whistler signals and their comparison with positions of lightning strokes [*Holzworth et al.*, 1999, and references therein]. Similar comparisons based on the spacecraft data have been recently done by *Chum et al.* [2006], who also showed that the area in the ionosphere through which the whistlers propagate is up to several thousands of kilometers wide.

[7] Ray-tracing methods have been extensively used in the past to study the propagation of whistlers in the ionosphere and magnetosphere. On the basis of the early ray-tracing results of *Kimura* [1966], a terminology for describing whistlers observed in space has been introduced by *Smith and Angerami* [1968]; a whistler that directly propagates to the satellite without crossing the magnetic equator is called a "0_+" whistler or, occasionally, a short fractional hop whistler. It is mostly accepted that the fractional-hop whistlers propagate through the ionosphere unducted [*Hughes*, 1981; *Hughes and Rice*, 1997], until they eventually can enter into the ducts at higher altitudes (1000–2000 km) [e.g., *James*, 1972]. Studies of lightning-induced electron precipitation (LEP) events [e.g., *Peter and Inan*, 2004] have shown that unducted propagation is common also at higher altitudes and in the magnetosphere. Most of these past studies used forward ray tracing of whistlers from their source to simulate observed spectrograms [e.g., *Kimura*, 1985; *Holzworth et al.*, 1999; *Shklyar and Jiricek*, 2000; *Shklyar et al.*, 2004; *Platino et al.*, 2005] or wave vector directions [e.g., *James*, 1972]. Only a few studies in the past were based on determination of wave vector or Poynting vector directions of whistlers using spacecraft measurements [*Gurnett et al.*, 1971; *James*, 1972; *Santolík and Parrot*, 1999; *Karlsson et al.*, 2005].

[8] In the present paper we, for the first time, combine spacecraft measurements of wave vector and Poynting vector directions of fractional-hop whistlers with backward ray tracing. This will allow us to determine the location and wave vector of each whistler when it penetrates upward into the ionosphere. We will use measurements of fractional-hop whistlers by the low-orbiting DEMETER satellite which carries unique instrumentation for multicomponent measurements of plasma waves and we will compare these results with ground-based observations of the source lightning strokes and atmospherics. The backward ray-tracing procedure, together with measured dispersions of the fractional-hop whistlers and ground-based ionosonde measurements, will also allow us to estimate the density profile in the topside ionosphere.

[9] In section 2 we describe the data sets and analysis methods, section 3 shows results of a case study of fractional-hop whistlers and their source lightning strokes, section 4 presents results of multicomponent propagation analysis for the selected cases, section 5 then describes results of reverse ray tracing down to the base of the ionosphere, and section 6 discusses the ionospheric density profile. Finally, section 7 contains brief conclusions.

2. Data Set and Data Processing

2.1. Spacecraft Measurements

[10] DEMETER is a low-altitude satellite launched in June 2004 into a polar Sun-synchronous orbit. The spacecraft carries a comprehensive set of scientific instruments, including devices which measure electromagnetic waves in plasmas surrounding the Earth at an altitude of ≈ 700 km and at low and middle latitudes. The frequency range is from DC up to 3.5 MHz for the electric field measurements [*Berthelier et al.*, 2006b], and between a few Hz up to 20 kHz for the magnetic field measurements [*Parrot et al.*, 2006]. There are two scientific modes. In the VLF range survey mode spectra of one electric and one magnetic component are computed onboard up to 20 kHz and burst mode waveforms of one electric field component and one magnetic field component are recorded up to 20 kHz. In the ELF range waveforms of three electric and three magnetic components are available up to 1.25 kHz in a burst mode. The burst mode data will be used in this case study, allowing us to perform spectral analysis with ideal time and frequency resolution in the VLF range and to analyze wave polarization and propagation characteristics in the ELF range [*Santolík et al.*, 2006b]. We will analyze fractional-hop whistlers recorded on 28 July 2005 during local late evening hours, when the spacecraft moved in its orbit above the Mediterranean sea to Southern France.

2.2. Ground-Based Measurements

[11] To detect atmospherics that are connected to the observed whistlers we will use ground-based radio recordings. The VLF receiver in Nançay, France (geographic coordinates: 2.1°E, 47.2°N.) is a part of a global network of ELF/VLF receivers (US, Japan, Greece, Turkey, Ireland, India) installed by Stanford University. The Nançay receiver uses a square air-core magnetic loop antenna of 2 meters in size. Its sensitivity allows us to measure magnetic fields as low as several tens of femtoTesla per root Hz, in the frequency range between 30 Hz and 50 kHz. In this study

we use measurements recorded during the DEMETER burst mode interval on 28 July 2005.

[12] As an additional data source we use ground-based measurements from the French lightning detection network METEORAGE. For comparison with satellite and ground-based measurements of lightning-generated electromagnetic waves in the VLF and ELF range we use data on position and peak current of the source lightning strokes determined from simultaneous high-frequency measurements by METEORAGE.

[13] Since the propagation of VLF/ELF electromagnetic waves to the satellite is strongly influenced by the ionosphere we also use information on the ionospheric density profile. We combine ground-based data of the ionosonde at the Ebro observatory in Spain (geographic coordinates: 0.5°E, 40.8°N) with the IRI-2007 ionospheric model [*Bilitza and Reinisch*, 2008].

2.3. Wave Propagation Analysis Methods

[14] We use several analysis methods to characterize the wave polarization and propagation from multicomponent measurements. All these methods are based on the spectral analysis of fluctuating electric and magnetic fields yielding a spectral matrix for every given time and frequency interval. The main diagonal of this Hermitian matrix contains information on wave power while the off-diagonal terms describe the phase and coherency relations between components. Supposing the presence of a single plane wave at each frequency f, we can use Faraday's law to find the wave vector $\mathbf{k}$ [*Santolík et al.*, 2006b].

[15] This leads us to an overdetermined set of equations with components of the spectral matrix 6×6 for 3 magnetic and 3 electric field components. We use a Singular Value Decomposition (SVD) technique to estimate a solution to this set. At a given frequency f, we obtain an estimate of the wave vector $\mathbf{k}$ in the "least squares" sense, taking into account all the experimentally determined components of the spectral matrix (for more details, see *Santolík et al.* [2003], equation (22)). We define it in a physical coordinate system locally linked to the ambient terrestrial magnetic field $\mathbf{B}_0$, where the z axis is parallel to $\mathbf{B}_0$, the x axis lies in the plane of the local magnetic meridian and points outward from the Earth, and the y axis completes the Cartesian system, pointing to the East. Using equation (9) of *Santolík et al.* [2003] we can then define the resulting wave vector direction by an angle θ between 0° and 180°, measuring inclination of the wave vector from $\mathbf{B}_0$ (polar angle with respect to the z axis), and by an azimuthal angle ϕ between −180° and +180°, measured from the x axis.

[16] Similar SVD technique, when applied only to magnetic components of the spectral matrix, also allows us to directly estimate the lengths and directions of the three axes of the polarization ellipsoid of magnetic field fluctuations [*Santolík et al.*, 2003]. Here we use the ratio of the longest axis to the medium axis L_p [*Santolík et al.*, 2003, equation (13)]. It varies between 0 (linear polarization) and 1 (circular polarization). We combine its value with the sense of the magnetic polarization with respect to $\mathbf{B}_0$, defining thus the ellipticity of the polarization to be $\ell = L_s\, L_p$ [see Appendix of *Santolík et al.*, 2002]. Here, L_s is −1 when the polarization is left handed (in the sense of the ion cyclotron motion), and L_s is +1 for right-handed polarization (in the sense of the electron cyclotron motion). For linear polarization, ℓ is zero.

[17] We also use another, more robust estimator of the propagation properties based on Cartesian components of the Poynting flux in the above described coordinate system linked to the ambient terrestrial magnetic field $\mathbf{B}_0$. A generalized form of equation (8) of *Santolík et al.* [2001] gives estimates of the components of the Poynting flux normalized by their standard deviations. These estimates are obtained from the components of the experimental spectral matrix and their standard deviations based on statistical properties of spectral analysis.

2.4. Ray-Tracing Simulation Method

[18] To analyze the propagation of the observed whistler waves through the ionosphere we follow the wave rays backward from the spacecraft position. This procedure is initialized by an experimentally estimated wave vector direction $\mathbf{k}_0/k_0$ at the spacecraft position $\mathbf{x}_0$.

[19] Under the approximation of the geometric optics, we then calculate the position $\mathbf{x}$ of a wave packet and its wave vector $\mathbf{k}$ as a function of the group time t_g. We use a modified version of the ray-tracing procedure of *Santolík et al.* [2006a] which has been rewritten with substantial updates and modifications based on the original 3-D technique of *Cerisier* [1970] and *Cairó and Lefeuvre* [1986]. The Wentzel-Krammers-Brillouin (WKB) approximation of the geometric optics represents the basic limitation or this method [*Budden*, 1988, p. 178; *Swanson*, 1989, p. 236]. It limits the dispersive properties of the medium to slowly varying functions of space compared to the wavelength. This approximation fails if the refractive index rapidly changes, near cutoffs, resonances, and sharp gradients of plasma parameters. Our modified procedure uses a numerical integration of differential equations for $\mathbf{x}$ and $\mathbf{k}$ by the fourth-order Runge-Kutta method with one midpoint and with an adaptive integration step. We stop the integration whenever the limit of the WKB approximation is encountered. In our procedure, this is coupled with adjusting the numerical integration step. The procedure is as follows: (1) during the numerical integration, we keep the relative variation of the wave vector, $|\mathbf{k}_i - \mathbf{k}_{i-1}|/k$, in a predefined interval between 10^{-4} and 10^{-3} by, respectively, decreasing or increasing the ith step ($i = 1,2,\ldots$) in the group time t_g; (2) ray tracing stops if the corresponding spatial step is small, which means if $|\mathbf{x}_i - \mathbf{x}_{i-1}|/L$ falls below $10^{-3}/\pi$, where $L = 2\pi/k$ is the wavelength.

[20] The method needs a realistic description of the magnetic field and plasma at any point along the obtained ray. We use the International Geomagnetic Reference Field (IGRF) model, and a diffusive equilibrium (DE) model of the plasma medium. Our DE model has several adjustable parameters, defining the height of the ionospheric F layer, the effective temperature, the ion composition and plasma density in a predefined height.

3. Spacecraft and Ground-Based Observations of Fractional-Hop Whistlers and Their Source Lightning

[21] On 28 July 2005, a storm system above France generated lightning strokes which, in turn, emitted electro-

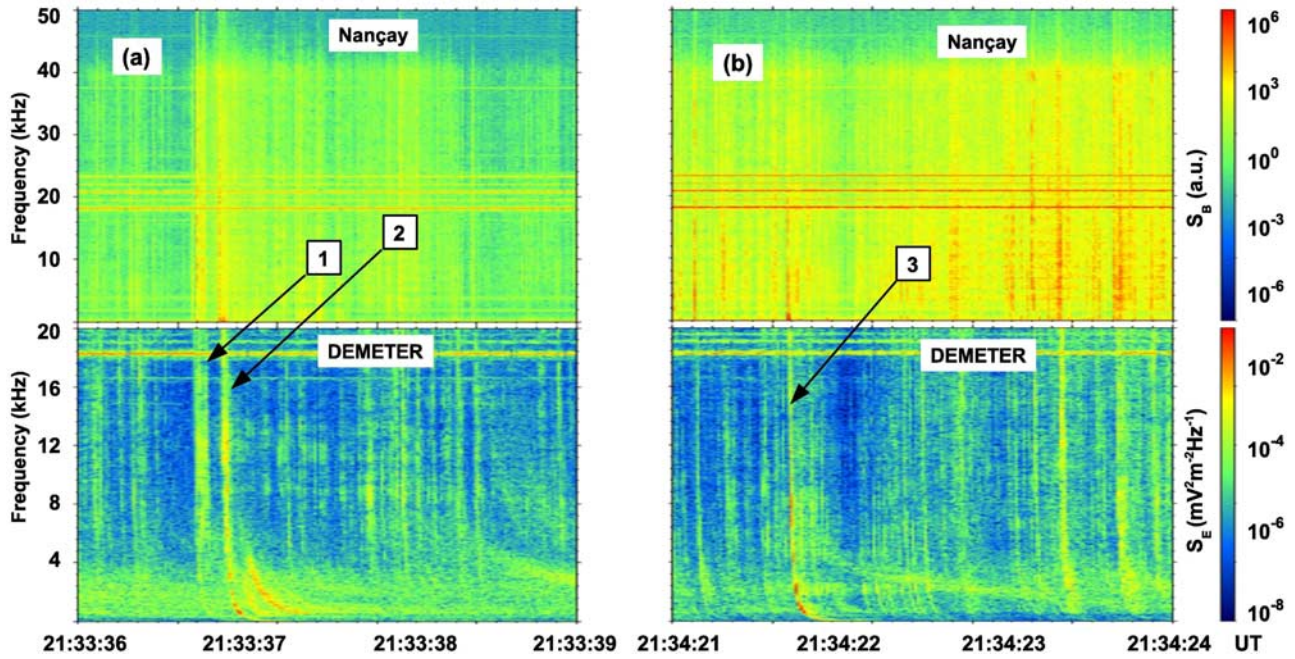

Figure 1. (a) Power spectrogram of the magnetic field measured at the Stanford VLF ground-based station in Nançay (France) on 28 July 2005 during 3 s after 2133:36 UT and power spectrogram of the electric field measured by the DEMETER spacecraft. Arrows show whistlers where the position and peak current of the source lightning are known from the data of the METEORAGE network. (b) The same for a 3-s time interval on 28 July 2005 after 2134:21 UT.

magnetic radiation propagating in the Earth-ionosphere waveguide. The top plots of Figures 1a and 1b show examples of measurements of this radiation by the ground-based station in Nançay. Frequency-time power spectrograms have been obtained by a frequency analysis of 3 s of received magnetic field waveform data, starting at 2133:36 UT, and 2134:21 UT, in Figures 1a and 1b, respectively. We have observed a large number of atmospherics, shown as vertical lines in the power spectrograms. (Note that the horizontal lines in the vicinity of 20 kHz are man-made signals originating from submarine navigation systems in France and UK.)

[22] During exactly identical time intervals, DEMETER overflew the Mediterranean region and observed fractional-hop whistlers. These whistlers originated from the same atmospherics, as are those observed by the Nançay station, as a result of penetration of a part of their electromagnetic energy from the Earth-ionosphere waveguide upward, through the ionosphere. Frequency-time power spectrograms obtained by a frequency analysis of received burst mode electric field waveforms in the VLF frequency range are shown in the bottom plots of Figures 1a and 1b. We can notice that most of the observed whistlers have their exact counterparts in the atmospherics observed on the ground, although the ratio of their intensities vary from case to case. Three strong events are highlighted by arrows in Figures 1a and 1b. The frequency-time dispersion of these fractional-hop whistlers is clearly apparent at lower frequencies for event 2 in Figure 1a and event 3 in Figure 1b. Event 2 additionally shows other more dispersed whistler traces immediately following the original fractional-hop whistler. The dispersion of these additional traces is too low for an explanation based on ducted propagation of whistler mode waves all the way through the magnetosphere with the reflection in the opposite hemisphere. These additional traces have been previously described as subprotonospheric whistlers [e.g., *Carpenter et al.*, 1964; *Gurnett et al.*, 1971] and are analyzed in a companion paper [*Chum et al.*, 2009].

[23] For the three marked events of coupled pairs of intense whistlers and atmospherics we have used the data from the METEORAGE lightning detection network to determine positions of source lightning strokes and peak currents. Event 1 in Figure 1a was caused by a negative peak current of −19.4 kA in a lightning discharge located in central France at a longitude of 2.53°E, and a latitude of 47.57°N. In the same Figure 1a, just 180 ms later, event 2 corresponds to another lightning discharge with a larger positive peak current of 97.0 kA, very close to the previous one at 2.58°E, and 47.57°N. Finally, event 3 in Figure 1b corresponds to a discharge with a positive peak current of 56.2 kA. This lightning occurred more to the South, in the Pyrenees, at geographical coordinates of 1.01°E and 42.58°N.

[24] This is illustrated by Figure 2a (for events 1 and 2) and by Figure 2b (for event 3) showing geographical maps and indicating the positions of DEMETER, of the Nançay station, and of the source lighting discharges. Note that the intensities of the atmospherics for events 1 and 2 are high since the Nançay observatory was very close to the source lightning flashes. On the other hand, we observe relatively weaker fractional-hop whistlers on DEMETER, approximately 1000 km to the South from the lightning strokes. This is a completely opposite situation compared to event 3, when DEMETER is close to the lightning flash and Nançay

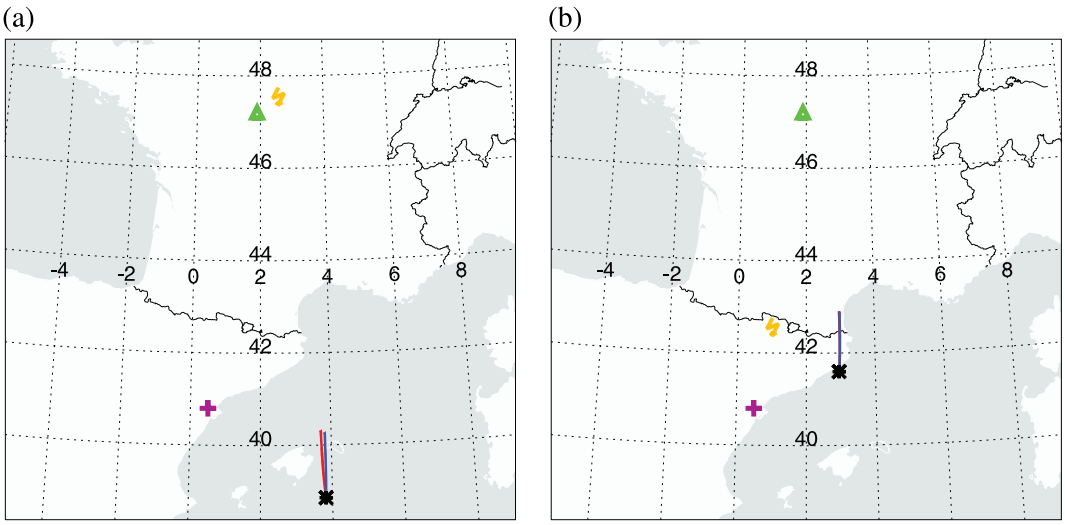

Figure 2. Maps illustrating (a) events 1 and 2 from Figure 1a and (b) event 3 from Figure 1b. The maps show, in geographic coordinates, positions of the source lightning strokes (yellow lightning symbols), the Nançay ground station in France (triangle symbol), the DEMETER spacecraft (black asterisk symbol), the reconstructed wave rays (short lines originating at the DEMETER position; see section 5), and position of the ionosonde at the Ebro observatory in Spain (plus symbol; see section 6).

is approximately 450 km further North. Indeed we observe a weak atmospheric at Nançay and stronger whistler on DEMETER. These observations support previous findings that the atmospherics can travel thousands of km in the Earth-ionosphere waveguide before releasing a part of their energy into the ionosphere, or in other words, that the region through which a whistler penetrates upward into the ionosphere is a few thousands of km wide.

4. Analysis of Multidimensional Measurements of Fractional-Hop Whistlers

[25] Figure 3 shows results of analysis of the waveforms of 3 magnetic field components and 3 electric field components recorded as burst mode ELF data in a 2-s time interval around events 1 and 2. Figures 3a and 3b, respectively, represent high-resolution power spectrograms of magnetic and electric field fluctuations. Both power spectrograms show the dispersed lower-frequency part of fractional-hop whistlers, much stronger for event 2. Event 2 is additionally followed by several traces of subprotonospheric whistlers with higher dispersion. Both events 1 and 2 are furthermore connected with proton whistlers [*Gurnett et al.*, 1965] with opposite dispersion, increasing their frequency with time and asymptotically approaching the proton cyclotron frequency.

[26] Figure 3c shows the ellipticity ℓ of the magnetic field polarization combined with the sense of polarization (see section 2.3). Note that results in Figure 3c, and in the following Figures 3d–3g are not plotted if the power spectral density of the magnetic field fluctuations (as shown in Figure 3a) is below a predefined threshold of 3×10^{-7} nT^2 Hz^{-1}. The obtained values of ℓ confirm that the fractional-hop electron whistlers are nearly circularly right-hand polarized (positive values close to 1), while the proton whistlers are left-hand polarized (negative values). The subprotonospheric whistlers following event 2 have right-hand elliptical polarization.

[27] Wave vector directions presented in Figures 3d and 3e have been obtained by the SVD method in the coordinate system linked to the ambient terrestrial magnetic field $\mathbf{B}_0$ (see section 2.3). The polar angle θ shows that both the fractional hop electron whistlers and the proton whistlers propagate upward with wave vectors at angles between 30° and 40° from $\mathbf{B}_0$, while the subprotonospheric whistlers are at angles around 90°. This is consistent with the observed elliptical polarization which can be expected for the whistler mode at high θ. The azimuth ϕ is around 0° for the fractional hop electron whistlers and the proton whistlers which means that the waves propagate in the plane of the local magnetic meridian with wave vectors inclined from $\mathbf{B}_0$ in the direction outward from the Earth. On the other hand, the subprotonospheric whistlers at ϕ around 180° have wave vectors inclined from $\mathbf{B}_0$ toward the Earth in the same plane. We find no signs of the precession of the polarization plane, as was observed for another case by *Karlsson et al.* [2005].

[28] Figures 3f and 3g represent results of a different method to determine how the waves propagate, based on the Poynting vector (see section 2.3). These results independently confirm the propagation characteristics, as they have been obtained from wave vector directions. The only distinction is that the measurements of the parallel component of the Poynting flux are able to resolve the downward propagation in the first trace of the subprotonospheric whistlers right after event 2. This is consistent with previous Poynting flux results obtained for subprotonospheric whistlers by *Gurnett et al.* [1971].

[29] Figure 4 shows the same parameters for event 3. Both the fractional-hop electron whistler and the associated proton whistler are stronger compared to events 1 and 2, but the propagation characteristics are very similar. This is also true for weak subprotonospheric whistlers immediately

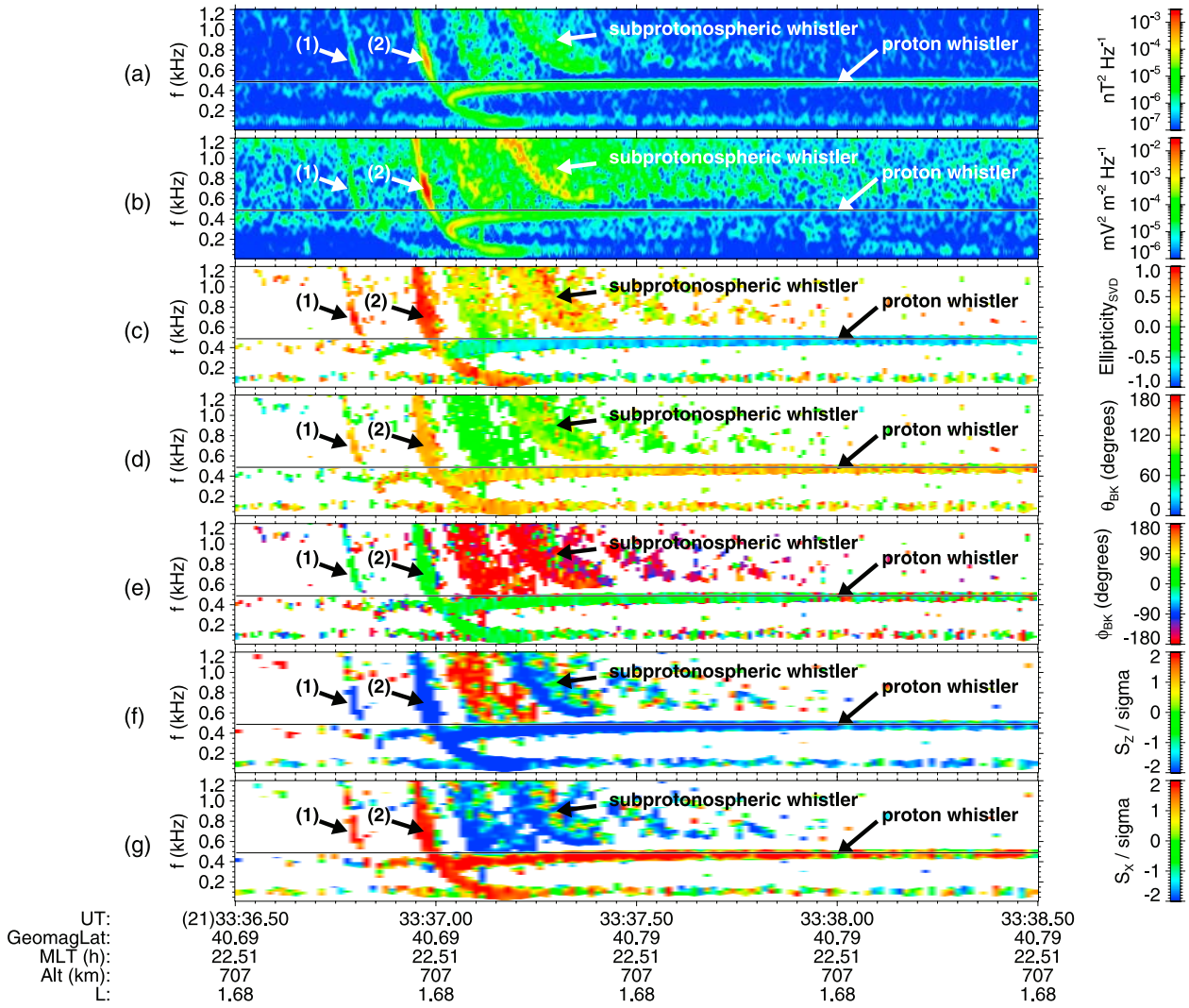

Figure 3. Results of analysis of the burst mode ELF data from DEMETER for events 1 and 2 from Figure 1a, indicated by arrows. (a) Power spectrogram of magnetic field fluctuations; (b) power spectrogram of electric field fluctuations; (c) ellipticity of the magnetic field polarization combined with the sense of polarization, positive for the right-hand sense, negative for the left-handed polarization; (d) polar angle of the wave vector with respect to the local field line of the terrestrial magnetic field; (e) azimuth of the wave vector with respect to the local field line; (f) sign estimator for the component of the Poynting flux parallel to $\mathbf{B}_0$; and (g) the same for the perpendicular component of the Poynting flux in the plane of the magnetic meridian. Black horizontal lines in Figures 3a–3g indicate the local proton cyclotron frequency. Geomagnetic latitude, magnetic local time (MLT), altitude (Alt), and the McIlwain's parameter (L).

following the fractional-hop whistler but propagating with different wave vectors. Again, we find no indications of the precession of the polarization plane observed by *Karlsson et al.* [2005].

5. Reverse Ray-Tracing Simulation Based on the Measured Wave Vector Directions

[30] The obtained wave vector directions from Figures 3 and 4 can be used as initial values for the three-dimensional ray-tracing procedure described in section 2.4. In this analysis we will only concentrate on propagation of strong fractional-hop electron whistlers, events 2 and 3. Other observed fractional-hop whistlers (for instance, event 1) show similar results of the propagation analysis. Ray-tracing analysis of subprotonospheric whistlers is beyond the scope of this paper but similar cases of subprotonospheric whistlers observed by DEMETER are analyzed in detail by *Chum et al.* [2009].

[31] To characterize the propagation of fractional-hop whistlers, we have selected two frequencies, 200 Hz and 700 Hz. Analysis presented in Figures 3d and 3e gives, for event 2, initial values of $\theta = 150°$, $\phi = 8°$ at 200 Hz and $\theta = 143°$, $\phi = -4°$ at 700 Hz. Results of the reverse ray-tracing simulation for these initial values are represented in Figure 5a which shows projections of the ray trajectories to the

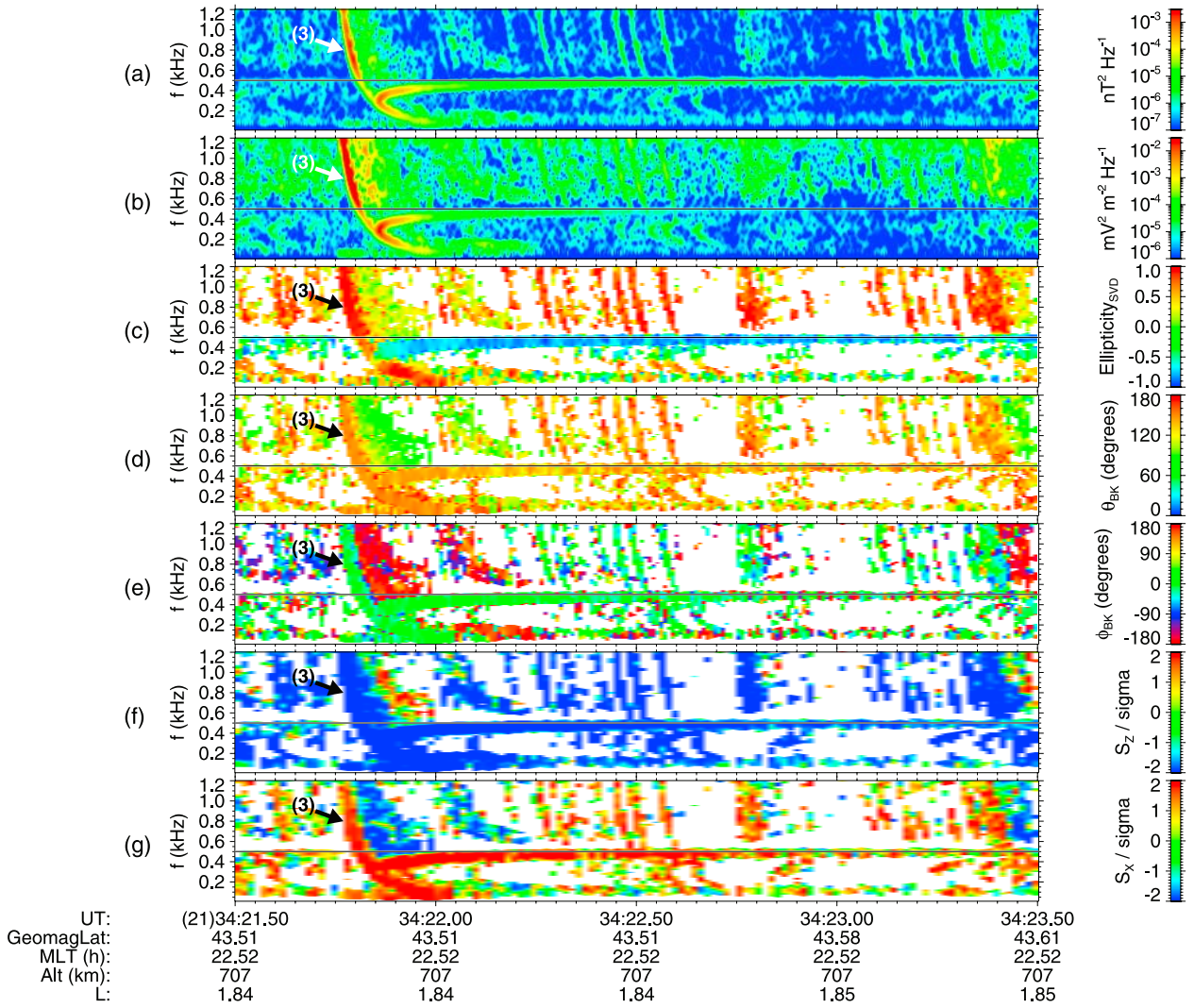

Figure 4. The same as in Figure 3 but for a different time interval comprising event 3 from Figure 1b, indicated by an arrow.

magnetic meridian plane, starting at the spacecraft position at an altitude of 707 km.

[32] At 200 Hz, the wave vector is inclined by an angle of 7.7° from the upward vertical direction at the spacecraft position. We follow the ray downward until the WKB approximation becomes invalid at the sharp plasma density drop on the bottom edge of the ionospheric F layer. This happens approximately 163 km to the North from the point vertically below the spacecraft (see also the vertical projections of the rays in Figure 2a), at an altitude of 214 km. This altitude level can be considered as the upper side of the interface between the ionosphere and the subionospheric waveguide. The wave vector direction at this level allows us to directly test the original assumptions of *Helliwell* [1965] on upward penetration of whistlers into the ionosphere. The resulting wave vector is here indeed very close to the upward vertical direction, only inclined by an angle α = 0.7°, with a refractive index N = 57 (a wavelength of 26 km) at this level for the whistler wave at 200 Hz.

[33] We thus find that the observed wave vector direction can be reasonably explained by using Snell's law for a simplified interface in the form of a horizontal plane below which the refractive index drops down to ≈1,

$$N \sin\alpha = \sin\alpha',$$

where α' is the angle of the wave vector with respect to the vertical on the bottomside of the interface, α being similar angle but on the topside of the interface, and N being the topside refractive index. The condition $\sin\alpha' \leq 1$ gives $\alpha \leq 1°$, which is clearly well satisfied in our case. Using the values obtained from our reverse ray-tracing simulation (α = 0.7°, N = 57) we obtain $\alpha' \approx 44°$ with respect to the vertical.

[34] We obtain very similar final results for the reverse ray tracing at 700 Hz, as is also shown in Figure 5a. This time, the initial wave vector is only inclined by 2.5° from the upward vertical direction at the spacecraft position. However, at the altitude level of 211 km, where the WKB approximation becomes invalid, we again obtain nearly vertical wave vectors inclined by α = 1.0°. This is consistent with Snell's law at the ionospheric interface, having the

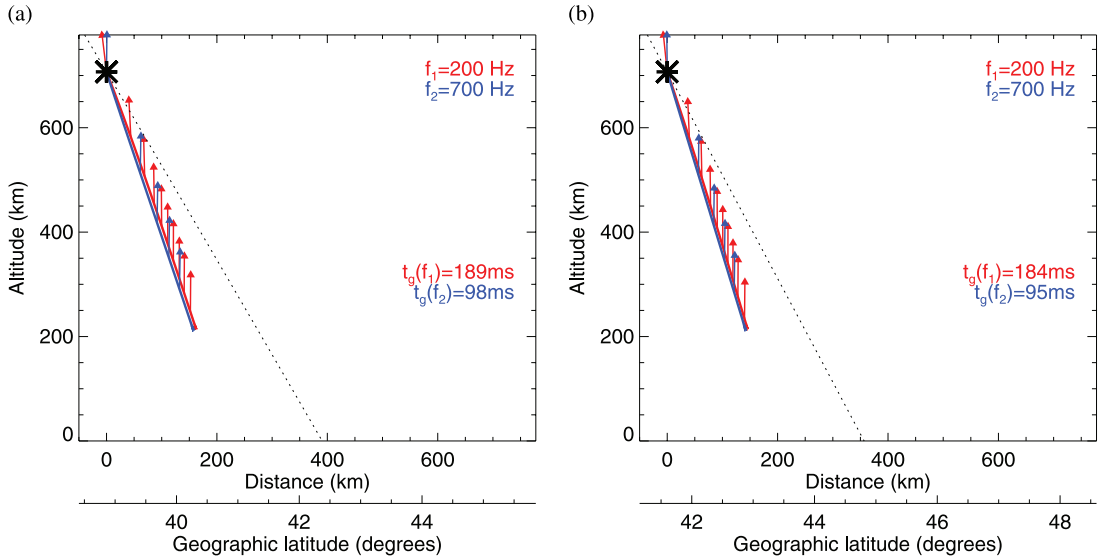

Figure 5. Reverse ray-tracing simulation based on the measured wave vector directions from Figures 3 and 4 for (a) event 2 and (b) event 3. The rays are plotted in the plane of the local geographic meridian starting at the DEMETER altitude (a black symbol) for two different frequencies of (red) 200 Hz (blue) 700 Hz. Arrows show the obtained wave vector directions plotted at fixed intervals of 20 ms of the group time. Dashed line represents the magnetic field line passing through the spacecraft position.

refractive index of $N = 23$ (a wavelength of 19 km) and obtaining $\alpha \leq 2.5°$.

[35] For event 3 we obtain initial values of $\theta = 152°$ $\phi = -8°$ and $\theta = 147°$ $\phi = -8°$, at 200 Hz and 700 Hz, respectively. Results of the reverse ray-tracing simulation are shown in Figure 2b as a projection of wave rays to the ground, and in Figure 5b as their projection to the plane of the local magnetic meridian. Although the relative positions of the source lightning stroke and the spacecraft are different compared to event 2, the ray-tracing results are very similar. At 200 Hz, the wave vector is initially shifted by 6.6° from the vertical, while we again obtain $\alpha = 0.5°$ with a refractive index $N = 55$ at an altitude of 213 km where the WKB approximation becomes invalid. At 700 Hz, the wave vector shifts from an inclination of 4.4° down to $\alpha = 0.8°$ at 211 km where $N = 23$. The conditions of Snell's law are again clearly well satisfied in this case, as is true in several other cases of DEMETER measurements of fractional-hop whistlers (not shown) that we have used for verification.

6. Models of Ionospheric Plasma Density Profiles: Topside Sounding by Whistlers

[36] The fractional-hop whistlers in Figures 3 and 4 show the typical dispersion owing to differences in propagation time at different frequencies. Within experimental uncertainties, both events 2 and 3 show the same delay of 91 ± 5 ms in propagation time between frequencies $f_2 = 700$ Hz and $f_1 = 200$ Hz. This delay must correspond to the difference of group times $t_g(f_1) - t_g(f_2)$ obtained from the ray-tracing simulations. Since the group time at a given frequency strongly depends on the model of the density profile through which the waves propagate, the measured delay can be used to estimate properties of the ionospheric density profile.

[37] The IRI-2007 model [*Bilitza and Reinisch*, 2008] provides us, for the given spacecraft position, with a density profile shown by the dotted line in Figure 6. As options of this model we have used the URSI F peak model and the corrected IRI-2001 model for the topside density. We have also tested the NeQuick topside model, with similar results as we describe below. The Ebro observatory in Spain, located close to the DEMETER position (see Figure 2), measured the electron density profiles shown by the cross ("X") and plus symbols in Figure 6. These digital ionosonde measurements give consistent results for two ionospheric soundings preceding our whistler recordings. The maximum of the *F* layer at an altitude of 300 km and with a peak density of 3-4 $\times$ 10^5 cm^{-3} coincides with the IRI model. However, the lower edge of the *F* layer, as found by the sounding measurements, is located higher compared to the IRI model, above an altitude of 200 km.

[38] To test the sensitivity of group times obtained from the ray-tracing simulations to the shape of the modeled density profile, we have first adjusted the parameters of the diffusive equilibrium (DE) model to fit the IRI profile. This gives the lower edge of the *F* layer at an altitude of 170 km. In our DE model we also need to define a single value for the effective temperature. In reality, the temperature depends on the altitude, we thus need to find a value of the effective temperature between the ion temperature of 920 K at the peak of the *F* layer in the IRI profile, and the ion temperature of 1630 K at the DEMETER altitude of 707 km, resulting in an effective temperature of 1030 K. With this value, the simplified DE model then gives a density profile which is very close to the IRI model, with a plasma density of 3 $\times$ 10^4 cm^{-3} at the DEMETER altitude. The resulting simulated group delay between frequencies of 700 Hz and 200 Hz is 110 ms for event 2. This is longer than the observed value. To fit both the ionosonde data and the topside IRI profile we need to increase the altitude of the

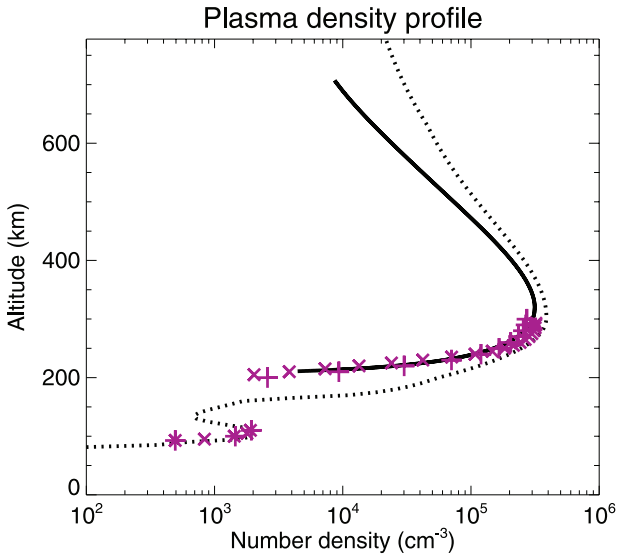

Figure 6. Measurements and models of ionospheric density profile as a function of altitude. The cross ("X") and plus symbols show the ionosonde measurements done from the Ebro observatory on 28 July 2005 at 2115:05 UT and at 2130:05 UT, respectively. The dotted line represents the IRI 2007 model [*Bilitza and Reinisch*, 2008]. The solid line shows the diffusive equilibrium model used by the ray-tracing procedure.

lower edge of the *F* layer to an observed altitude of 205 km, and decrease the temperature to 930 K. Nevertheless, the resulting group delay is still too high, 105 ms.

[39] The total integrated density along the rays must be lower to give the model group delay close to the observed delay of 91 ms. Since the ionosonde profile is a result of direct measurements we need to modify the topside model. If we decrease the effective temperature to 700 K, lower than the ion temperatures predicted by the IRI model, the ray-tracing simulation gives a value of $t_g(f_1)-t_g(f_2) = 91$ ms which matches the observations. This model is shown by the solid line in Figure 6 and has been used for the ray-tracing simulations presented in Figures 2 and 5. For the event 3, we obtain $t_g(f_1)-t_g(f_2) = 89$ ms using the same ionospheric model. This is, within the range of experimental uncertainties, still consistent with the experimental value of 91 ms. The typical spatial scale for the density decrease in the topside ionosphere by a factor of $1/e$ (scale height) is then $\approx$100 km.

[40] This procedure shows that the measured dispersion and wave vector directions of fractional-hop whistlers can be successfully used for sounding of the topside ionosphere. Combined with results from ground-based ionosonde, these measurements lead us to estimation of the local density profile in the ionospheric *F* layer. With a given peak density in the *F* layer, the lower effective temperature results in a 3 times lower plasma density of 9×10^3 cm^{-3} at the DEMETER altitude compared to the IRI model.

[41] Direct measurements of the ion densities and temperatures have been done onboard DEMETER by the IAP instrument [*Berthelier et al.*, 2006a]. These measurements, processed by the method of *Séran* [2003], give a plasma density of 5.6×10^3 cm^{-3} (E. Séran, private communication, 2008) which is closer to our model value. Note that if we further decrease the effective temperature of the DE model to $\approx$650 K, we can obtain this lower plasma density at the spacecraft altitude and still stay approximately consistent with the measured whistler dispersion. This modification of the density model has no influence on the above

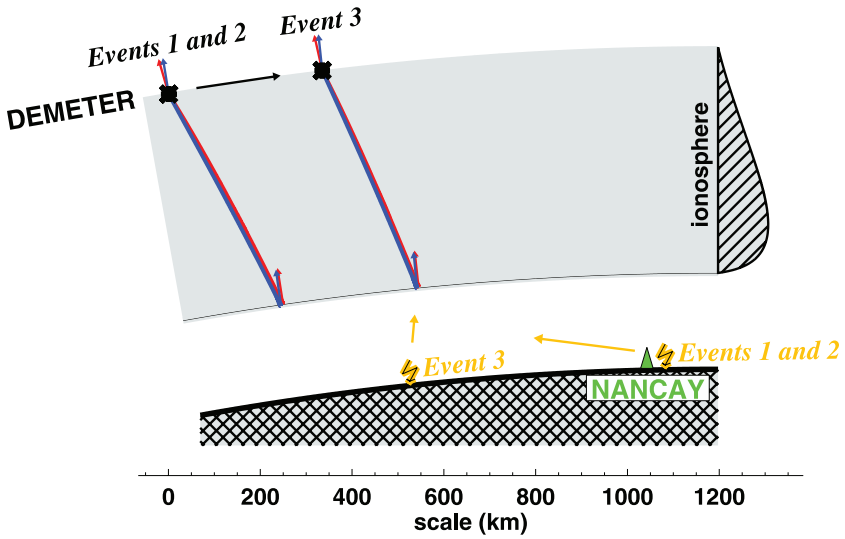

Figure 7. Summary plot showing the events described in the present paper. Positions of the source lightning strokes are projected on the plane of the geographic meridian of the ground-based VLF station in Nançay, France, at a longitude of 2.12°E. The fractional-hop whistler rays are projected on the same plane together with the wave vector directions obtained using the multicomponent measurements of the DEMETER spacecraft and with the calculated wave vector directions on the bottomside of the ionospheric *F* layer. The spatial scale of the plot is shown on the bottom. The profile of the logarithm of the ionospheric plasma density is schematically plotted on the right.

listed results. The ion temperature of 1400 K estimated from the IAP measurements is lower than the ion temperature in the IRI model at the DEMETER altitude (1630 K). This difference is consistent with a lower effective temperature in our DE model which fits the observed dispersion with respect to the effective temperature which fits the IRI model.

7. Conclusions

[42] The present paper represents, to our knowledge, the first attempt to use spacecraft measurements of wave vector and Poynting vector directions of fractional-hop whistlers as initial parameters for ray-tracing simulations. We analyze 3-D waveforms of the electric and magnetic fields of fractional-hop whistlers, which are recorded by the DEMETER spacecraft at 707 km of altitude, and which originate from lightning sources located in the same hemisphere as the spacecraft. The corresponding atmospherics are recorded by a VLF station located in Nançay (France) and the source lightning strokes are detected by the METEORAGE lightning detection network. We thus know the positions and parameters of the lightning sources of the whistler mode radiation observed by DEMETER in the topside ionosphere. Figure 7 presents a summary plot of the events that are described in the present paper, using the same scale for both horizontal and vertical distances.

[43] Multidimensional analysis of the DEMETER measurements provides us with wave polarization characteristics and propagation directions. We then use a backward ray-tracing technique to estimate ray paths of the fractional hop whistlers from their entry points into the ionosphere up to the spacecraft altitude. As a part of this procedure we present a method of topside sounding by fractional-hop whistlers. Their measured dispersion, combined with the ionosonde measurements at the Ebro observatory in Spain allows us to derive the density profile in the topside ionosphere.

[44] On the basis of the results of backward ray tracing of the observed fractional-hop whistlers we are able to show that their wave vector directions are very close to vertical just after they penetrate upward into the ionosphere, consistent with a simple model of planar discontinuity at the level of the bottomside of the ionospheric F layer. No effects similar to observations of precession of the normal to the polarization plane [*Karlsson et al.*, 2005] are found in the analyzed cases. The lightning detection data allow us to compare the obtained ray traces with the positions of their source lightning strokes. The upward penetration into the ionosphere occurs at distances of 100–900 km from the source lightning. The simultaneously observed atmospherics travel the same distance to the VLF ground station (see Figure 7). This suggests that the size of the upward penetration region represents a major contribution to the characteristic size of the region illuminated by whistlers returning to the ground after their reflection in the opposite hemisphere [*Storey*, 1953]. This is also consistent with previously published studies based on direct measurements of fractional-hop whistlers by *Holzworth et al.* [1999] and *Chum et al.* [2006]. An extensive ray-tracing study involving a large number of events is needed to confirm these results.

[45] **Acknowledgments.** We thank the CNES personnel involved in the mission development of the DEMETER satellite and those currently in charge of the operations in Toulouse. We thank J. J. Berthelier for the DEMETER IAP and ICE data. We acknowledge the digital Ionogram Database at CAR UMASS, Lowell, for the Ebro ionosonde data. We thank G. Diendorfer and the EUCLID network for lightning data used to verify identification of source discharges. We acknowledge discussions with E. Séran, and we thank her for her help with analysis of the IAP data. We acknowledge discussions of the IGRF model with V. Truhlík and L. Třísková. We acknowledge support of PICS grant 3725 from CNRS/DREI and of grant IAA301120601 from GAAV, and we thank the International Space Science Institute for supporting the meetings of the WFM team 89.

References

Akalin, F., D. A. Gurnett, T. F. Averkamp, A. M. Persoon, O. Santolik, W. S. Kurth, and G. B. Hospodarsky (2006), First whistler observed in the magnetosphere of Saturn, *Geophys. Res. Lett.*, *33*, L20107, doi:10.1029/2006GL027019.

Berthelier, J., M. Godefroy, F. Leblanc, E. Seran, D. Peschard, P. Gilbert, and J. Artru (2006a), IAP, the thermal plasma analyzer on DEMETER, *Planet. Space Sci.*, *54*, 487–501, doi:10.1016/j.pss.2005.10.018.

Berthelier, J., et al. (2006b), ICE, the electric field experiment on DEMETER, *Planet. Space Sci.*, *54*, 456–471, doi:10.1016/j.pss.2005.10.016.

Bilitza, D., and B. W. Reinisch (2008), International Reference Ionosphere 2007: Improvements and new parameters, *Adv. Space Res.*, *42*, 599–609, doi:10.1016/j.asr.2007.07.048.

Bortnik, J., U. S. Inan, and T. F. Bell (2003), Energy distribution and lifetime of magnetospherically reflecting whistlers in the plasmasphere, *J. Geophys. Res.*, *108*(A5), 1199, doi:10.1029/2002JA009316.

Bortnik, J., U. S. Inan, and T. F. Bell (2006), Temporal signatures of radiation belt electron precipitation induced by lightning-generated MR whistler waves: 2. Global signatures, *J. Geophys. Res.*, *111*, A02205, doi:10.1029/2005JA011398.

Bortnik, J., R. M. Thorne, and N. P. Meredith (2008), The unexpected origin of plasmaspheric hiss from discrete chorus emissions, *Nature*, *452*, 62–66, doi:10.1038/nature06741.

Budden, K. G. (1988), *The Propagation of Radio Waves*, Cambridge Univ. Press, New York.

Cairó, L., and F. Lefeuvre (1986), Localization of sources of ELF/VLF hiss observed in the magnetosphere: Three-dimensional ray tracing, *J. Geophys. Res.*, *91*, 4352–4364.

Carpenter, D. L. (1963), Whistler evidence of a "knee" in the magnetospheric ionization density profile, *J. Geophys. Res.*, *68*, 1675–1682.

Carpenter, D. L., N. Dunckel, and J. F. Walkup (1964), A new very low frequency phenomenon: Whistlers trapped below the protonosphere, *J. Geophys. Res.*, *69*, 5009–5017.

Cerisier, J. (1970), Propagation perpendiculaire au voisinage de la fréquence de la résonance hybride basse, in *Plasma Waves in Space and in the Laboratory*, vol. 2, pp. 487–521, Edinburgh Univ. Press, Edinburgh, U. K.

Chum, J., F. Jiricek, O. Santolik, M. Parrot, G. Diendorfer, and J. Fiser (2006), Assigning the causative lightning to the whistlers observed on satellites, *Ann. Geophys.*, *24*, 2921–2929.

Chum, J., O. Santolik, and M. Parrot (2009), Analysis of subprotonospheric whistlers observed by DEMETER: A case study, *J. Geophys. Res.*, *114*, A02307, doi:10.1029/2008JA013585.

Crary, J. H., R. A. Helliwell, and R. F. Chase (1956), Stanford-Seattle whistler observations, *J. Geophys. Res.*, *61*, 35–44.

Draganov, A. B., U. S. Inan, V. S. Sonwalkar, and T. F. Bell (1992), Magnetospherically reflected whistlers as a source of plasmaspheric hiss, *Geophys. Res. Lett.*, *19*, 233–236.

Ferencz, O. E., C. Ferencz, P. Steinbach, J. Lichtenberger, D. Hamar, M. Parrot, F. Lefeuvre, and J.-J. Berthelier (2007), The effect of subionospheric propagation on whistlers recorded by the DEMETER satellite—Observation and modelling, *Ann. Geophys.*, *25*, 1103–1112.

Green, J. L., S. Boardsen, L. Garcia, W. W. L. Taylor, S. F. Fung, and B. W. Reinisch (2005), On the origin of whistler mode radiation in the plasmasphere, *J. Geophys. Res.*, *110*, A03201, doi:10.1029/2004JA010495.

Green, J. L., S. Boardsen, L. Garcia, S. F. Fung, and B. W. Reinisch (2006), Reply to "Comment on 'On the origin of whistler mode radiation in the plasmasphere' by Green et al.," *J. Geophys. Res.*, *111*, A09211, doi:10.1029/2006JA011622.

Gurnett, D. A., S. D. Shawhan, N. M. Brice, and R. L. Smith (1965), Ion cyclotron whistlers, *J. Geophys. Res.*, *70*, 1665–1688.

Gurnett, D. A., S. R. Mosier, and R. R. Anderson (1971), Color spectrograms of very-low-frequency Poynting flux data, *J. Geophys. Res.*, *76*, 3022–3033, doi:10.1029/JA076i013p03022.

Gurnett, D. A., R. R. Shaw, R. R. Anderson, and W. S. Kurth (1979), Whistlers observed by Voyager 1: Detection of lightning on Jupiter, *Geophys. Res. Lett.*, *6*, 511–514.

Gurnett, D. A., P. Zarka, R. Manning, W. S. Kurth, G. B. Hospodarsky, T. F. Averkamp, M. L. Kaiser, and W. M. Farrell (2001), Non-detection at Venus of high-frequency radio signals characteristic of terrestrial lightning, *Nature*, *409*, 313–315.

Helliwell, R. (1965), *Whistlers and Related Ionospheric Phenomena*, Stanford Univ. Press, Stanford, Calif.

Helliwell, R. (1993), 40 years of whistlers, in *Modern Radio Science 1993*, edited by H. Matsumoto, pp. 189–212, Oxford Univ. Press, New York.

Helliwell, R. A., J. H. Crary, J. H. Pope, and R. L. Smith (1956), The "NOSE" WHISTLER—A new high-latitude phenomenon, *J. Geophys. Res.*, *61*, 139–142, doi:10.1029/JZ061i001p00,139.

Holzworth, R. H., R. M. Winglee, B. H. Barnum, Y. Li, and M. C. Kelley (1999), Lightning whistler waves in the high-latitude magnetosphere, *J. Geophys. Res.*, *104*, 17,369–17,378, doi:10.1029/1999JA900160.

Hughes, A. R. W. (1981), Satellite measurements of whistler dispersion at low latitudes, *Adv. Space Res.*, *1*(1), 377–380, doi:10.1016/0273-1177(81)90138-1.

Hughes, A. R. W., and W. K. Rice (1997), A satellite study of low latitude electron and proton whistlers, *J. Atmos. Terr. Phys.*, *59*, 1217–1222.

Inan, U. S., D. Piddyachiy, W. B. Peter, J. A. Sauvaud, and M. Parrot (2007), DEMETER satellite observations of lightning-induced electron precipitation, *Geophys. Res. Lett.*, *34*, L07103, doi:10.1029/2006GL029238.

Iwai, A., T. Okada, and M. Hayakawa (1974), Rocket measurement of wave normal directions of low-latitude sunset whistlers, *J. Geophys. Res.*, *79*, 3870–3873, doi:10.1029/JA079i025p03870.

James, H. G. (1972), Refraction of whistler-mode waves by large-scale gradients in the middle-latitude ionosphere, *Ann. Geophys.*, *28*, 301–339.

Karlsson, R. L., T. D. Carozzi, J. E. S. Bergman, and A. I. Eriksson (2005), Precession of the whistler polarisation plane normal observed on Freja, *Geophys. Res. Lett.*, *32*, L23107, doi:10.1029/2005GL024748.

Kimura, I. (1966), Effects of ions on whistler-mode ray tracing, *Radio Sci.*, *1*, 269.

Kimura, I. (1985), Whistler mode propagation in the earth and planetary magnetospheres and ray tracing techniques, *Space Sci. Rev.*, *42*, 449–466.

McCormick, R. J., C. J. Rodger, and N. R. Thomson (2002), Reconsidering the effectiveness of quasi-static thunderstorm electric fields for whistler duct formation, *J. Geophys. Res.*, *107*(A11), 1396, doi:10.1029/2001JA009219.

Meredith, N. P., R. B. Horne, S. A. Glauert, and R. R. Anderson (2007), Slot region electron loss timescales due to plasmaspheric hiss and lightning-generated whistlers, *J. Geophys. Res.*, *112*, A08214, doi:10.1029/2007JA012413.

Ohta, K., A. Shimizu, and M. Hayakawa (1994), The effect of subionospheric propagation on whistlers as deduced from direction finding measurements, *Geophys. Res. Lett.*, *21*, 89–92.

Parrot, M., et al. (2006), The magnetic field experiment IMSC and its data processing onboard DEMETER: Scientific objectives, description and first results, *Planet. Space Sci.*, *54*, 512–527, doi:10.1016/j.pss.2005.10.015.

Pasmanik, D. L., and V. Y. Trakhtengerts (2005), Dispersion properties of ducted whistlers, generated by lightning discharge, *Ann. Geophys.*, *23*, 1433–1439.

Peter, W. B., and U. S. Inan (2004), On the occurrence and spatial extent of electron precipitation induced by oblique nonducted whistler waves, *J. Geophys. Res.*, *109*, A12215, doi:10.1029/2004JA010412.

Peter, W. B., and U. S. Inan (2007), A quantitative comparison of lightning-induced electron precipitation and VLF signal perturbations, *J. Geophys. Res.*, *112*, A12212, doi:10.1029/2006JA012165.

Platino, M., U. S. Inan, T. F. Bell, D. A. Gurnett, J. S. Pickett, P. Canu, and P. M. E. Décréau (2005), Whistlers observed by the Cluster spacecraft outside the plasmasphere, *J. Geophys. Res.*, *110*, A03212, doi:10.1029/2004JA010730.

Rodger, C. J., M. A. Clilverd, and R. J. McCormick (2003), Significance of lightning-generated whistlers to inner radiation belt electron lifetimes, *J. Geophys. Res.*, *108*(A12), 1462, doi:10.1029/2003JA009906.

Russell, C. T., T. L. Zhang, M. Delva, W. Magnes, R. J. Strangeway, and H. Y. Wei (2007), Lightning on Venus inferred from whistler-mode waves in the ionosphere, *Nature*, *450*, 661–662, doi:10.1038/nature05930.

Santolík, O., and M. Parrot (1999), Case studies on the wave propagation and polarization of ELF emissions observed by Freja around the local proton gyrofrequency, *J. Geophys. Res.*, *104*, 2459–2476, doi:10.1029/1998JA900045.

Santolík, O., F. Lefeuvre, M. Parrot, and J. Rauch (2001), Complete wave-vector directions of electromagnetic emissions: Application to Interball-2 measurements in the nightside auroral zone, *J. Geophys. Res.*, *106*, 13,191–13,201.

Santolík, O., J. S. Pickett, D. A. Gurnett, and L. R. O. Storey (2002), Magnetic component of narrowband ion cyclotron waves in the auroral zone, *J. Geophys. Res.*, *107*(A12), 1444, doi:10.1029/2001JA000146.

Santolík, O., M. Parrot, and F. Lefeuvre (2003), Singular value decomposition methods for wave propagation analysis, *Radio Sci.*, *38*(1), 1010, doi:10.1029/2000RS002523.

Santolík, O., J. Chum, M. Parrot, D. A. Gurnett, J. S. Pickett, and N. Cornilleau-Wehrlin (2006a), Propagation of whistler mode chorus to low altitudes: Spacecraft observations of structured ELF hiss, *J. Geophys. Res.*, *111*, A10208, doi:10.1029/2005JA011462.

Santolík, O., F. Nìmec, M. Parrot, D. Lagoutte, L. Madrias, and J. J. Berthelier (2006b), Analysis methods for multi-component wave measurements on board the DEMETER spacecraft, *Planet. Space Sci.*, *54*, 512–527.

Sazhin, S., M. Hayakawa, and K. Bullough (1992), Whistler diagnostics of magnetospheric parameters: A review, *Ann. Geophys.*, *10*, 293–308.

Séran, E. (2003), Reconstruction of the ion plasma parameters from the current measurements: Mathematical tool, *Ann. Geophys.*, *21*, 1159–1166.

Shklyar, D. R., and F. Jiricek (2000), Simulation of nonducted whistler spectrograms observed aboard the Magion 4 and 5 satellites, *J. Atmos. Space Phys.*, *62*, 347–370.

Shklyar, D. R., J. Chum, and F. Jiricek (2004), Characteristic properties of Nu whistlers as inferred from observations and numerical modelling, *Ann. Geophys.*, *22*, 3589–3606.

Smith, R. L., and J. J. Angerami (1968), Magnetospheric properties deduced from OGO 1 observations of ducted and nonducted whistlers, *J. Geophys. Res.*, *73*, 1–20.

Smith, R. L., and D. L. Carpenter (1961), Extension of Nose whistler analysis, *J. Geophys. Res.*, *66*, 2582–2586.

Sonwalkar, V. S., and U. S. Inan (1989), Lightning as an embryonic source of VLF hiss, *J. Geophys. Res.*, *94*, 6986–6994.

Storey, L. R. O. (1953), An investigation of whistling atmospherics, *Philos. Trans. R. Soc. London, Ser. A*, *246*, 113–141.

Swanson, D. G. (1989), *Plasma Waves*, Academic, San Diego, Calif.

Thorne, R. M., R. B. Horne, and N. P. Meredith (2006), Comment on "On the origin of whistler mode radiation in the plasmasphere" by Green et al., *J. Geophys. Res.*, *111*, A09210, doi:10.1029/2005JA011477.

D. Burešová and J. Chum, Department of Aeronomy, Institute of Atmospheric Physics, Boční II 1401, 141 31 Praha 4, Czech Republic. (buresd@ufa.cas.cz; jachu@ufa.cas.cz)

D. A. Gurnett, Department of Physics and Astronomy, University of Iowa, Iowa City, IA 52242-1479, USA. (donald-gurnett@uiowa.edu)

U. S. Inan, Space, Telecommunications and Radioscience Laboratory, Packard Building, Room 355, 350 Serra Mall, Stanford University, Stanford, CA 94305-9515, USA. (inan@stanford.edu)

M. Parrot, Laboratoire de Physique et Chimie de l'Environnement, CNRS, 3a Avenue de la Recherche Scientifique, F-45100 Orl'eans, France. (mparrot@cnrs-orleans.fr)

O. Santolík, Department of Space Physics, Institute of Atmospheric Physics, Boční II 1401, 141 31 Praha 4, Czech Republic. (ondrej.santolik@mff.cuni.cz)